Lift Generation and Streamline Curvature

Prof. David L. Darmofal
Department of Aeronautics and Astronautics
Massachusetts Institute of Technology

October 13, 2005

1 Objective

The objective of these notes is to explain how an airfoil generates lift using a streamline curvature analysis. The analysis will show in a qualitative manner how the shape of an airfoil influences the pressure distribution, and therefore the lift.

2 Inviscid Momentum in Natural Coordinates

The steady, two-dimensional momentum equations in (x, y) coordinates is,

$$\rho \vec{V} \cdot \nabla u = -\frac{\partial p}{\partial x}, \tag{1}$$

$$\rho \vec{V} \cdot \nabla v = -\frac{\partial p}{\partial y}, \tag{2}$$

where $\vec{V} = u\vec{i} + v\vec{j}$. Instead of an (x, y) coordinate system, these equations can be written in a stream-aligned coordinated system (r, s). As shown in Figure 1, r is the direction normal to the local streamwise direction and s is the local streamwise direction. In this coordinate system, the inviscid momentum equations are,

$$\rho V \frac{\partial V}{\partial s} = -\frac{\partial p}{\partial s}, \tag{3}$$

$$\rho \frac{V^2}{R} = \frac{\partial p}{\partial r}, \tag{4}$$
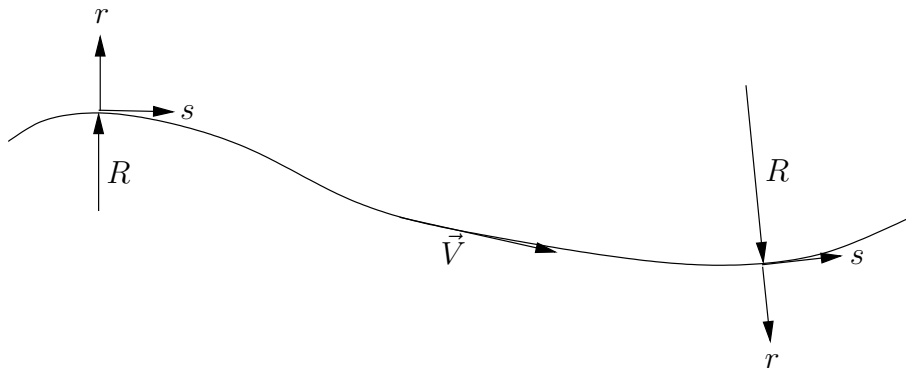
Figure 1: Natural coordinate system (r, s). r is the direction normal to the streamwise direction (along the radius of curvature), s is in the streamwise direction (tangent to the velocity vector, $\vec{V}$). R is the radius of curvature.
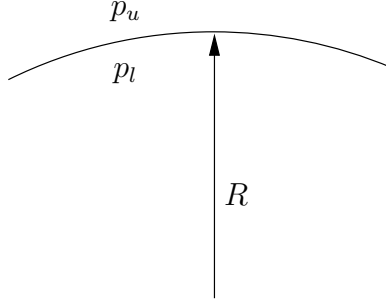
Figure 2: Airfoil with a circular arc camber line with radius R and zero thickness. p_u is the upper surface pressure, p_l is the lower surface pressure.

where $V = |\vec{V}|$ is the magnitude of the velocity vector (i.e. the speed).

For incompressible flow, we note that Equation (3) is equivalent to Bernoulli's equation,

$$\rho V \frac{\partial V}{\partial s} = -\frac{\partial p}{\partial s},$$

$$\frac{\partial}{\partial s}\left(\frac{1}{2}\rho V^2\right) = -\frac{\partial p}{\partial s},$$

$$\frac{\partial}{\partial s}\left(p + \frac{1}{2}\rho V^2\right) = 0,$$

$$p + \frac{1}{2}\rho V^2 = \text{constant}.$$

However, the key to understanding lift generation is not Bernoulli's equation (contrary to popular believe) but rather is the normal momentum equation, Equation (4).

3   Impact of Camber

The impact of camber on the pressure distributions can be demonstrated most simply by considering an airfoil with a circular arc camber line and zero thickness as shown in Figure 2. Far away from the airfoil, the pressure returns to the freestream pressure p_∞.

On the surface of the airfoil (which must be a streamline), we know that $\partial p/\partial r > 0$ from Equation (4). Thus, above the airfoil the pressure increases as the distance from the airfoil increases. Since the pressure must eventually return to p_∞, this implies that $p_u < p_\infty$. Summarizing the logic chain,

$$\frac{\partial p}{\partial r} = \rho \frac{V^2}{R} > 0 \Rightarrow p_\infty - p_u > 0 \Rightarrow p_u < p_\infty.$$

Similarly, on the lower surface,

$$\frac{\partial p}{\partial r} = \rho \frac{V^2}{R} > 0 \Rightarrow p_l - p_\infty > 0 \Rightarrow p_l > p_\infty.$$

Combining these results which are solely based on the curvature of the surface, we see that $p_u < p_\infty < p_l$. Thus, this airfoil will generate lift since the pressure is lower on the upper surface than on the lower surface.

As an example of the pressure distribution on a thin, circular arc airfoil, consider the NACA 4502 airfoil. This airfoil has a maximum thickness which is 2% of the chord length. The maximum camber is 4% of the chord and occurs at $x/c = 0.5$. Note: the NACA 4-digit series airfoils have camberlines which are two circular arcs that meet at the maximum camber location. Thus, when the maximum camber is at $x/c = 0.5$, the two circular arcs have the same radius. The c_p distribution for the 4502 at a $c_l = 0.5$ is shown in Figure 3. Recall the definition of c_p is,

$$c_p \equiv \frac{p - p_\infty}{\frac{1}{2}\rho_\infty V_\infty}. \tag{5}$$

Thus, when the pressure is below p_∞, $c_p < 0$ and vice-versa. The c_p distribution for the 4502 shows that the pressures are below p_∞ on the upper surface, and above p_∞ on the lower surface. Furthermore, the decrease in pressure on the upper surface is nearly equal to the increase in pressure on the lower surface which is reasonable since the radius of curvature is essentially the same on both the upper and lower surface.

Note that near the leading edge, the flow will have a stagnation point, $V = 0$. This corresponds to $c_p = 1$. However, in Figure 3, the c_p at the leading edge has a maximum value of about $c_p = 0.15$. The reason the stagnation point is not observed is purely numerical; the panel method does not have enough panels to resolve the leading-edge region. If the number of panels at the leading edge were increased, or the thickness of the airfoil were increased, then the leading-edge stagnation point would be better resolved.

As another example, Figure 4 shows the pressure distribution for a NACA 4202. This airfoil has a camber line with two different radius of curvatures; one from the leading edge until the maximum camber at $x/c = 0.2$ and the other from the maximum camber until the trailing edge. The radius of curvature is smaller from $x/c < 0.2$, thus the normal pressure gradients are generally expected to be larger in this region than for $x/c > 0.2$. This behavior is clearly observed in the c_p distribution. The magnitude of the c_p's drop abruptly for $x/c > 0.2$.

4   Impact of Thickness

The impact of thickness can also be explained qualitatively from streamline curvature arguments. Consider a symmetric airfoil with thickness. In this case, the curvature of the upper and lower surfaces are in opposite directions. Thus, the logic chain becomes,

$$\frac{\partial p}{\partial r} = \rho \frac{V^2}{R} > 0 \Rightarrow p_\infty - p_u > 0 \Rightarrow p_u < p_\infty.$$

Similarly, on the lower surface,

$$\frac{\partial p}{\partial r} = \rho \frac{V^2}{R} > 0 \Rightarrow p_\infty - p_l > 0 \Rightarrow p_l < p_\infty.$$

Thus, for a symmetric airfoil at zero angle of attack, the pressures on the surface are generally expected to be lower than p_∞. As examples of symmetric airfoils, the c_p distributions for NACA 0002 and 00010 airfoils at zero angle of attack are shown in Figures 5 and 6, respectively. The low pressures are observed on both surfaces (note: the flow is symmetric since the geometry is symmetric and $\alpha_\infty = 0$, thus the c_p on the upper and lower surfaces are the same). Also, the pressures are lower for the thicker airfoil as would be expected since the radius of curvature is small for the thicker airfoil.

On a camber airfoil, the trends with thickness are similar to the trends on a symmetric airfoil. Specifically, the addition of thickness will tend to lower the c_p on both size of the airfoil. Once again, this qualitative behavior can be motivated using streamline curvature arguments. Increasing the thickness on a cambered airfoil will tend to decrease the radius of curvature of the upper surface, and increase the radius of curvature of the lower surface. Thus, we have the following logic chain, on the upper surface,

$$\tau \uparrow \quad R \downarrow \quad \frac{\partial p}{\partial r} = \rho \frac{V^2}{R} \uparrow \quad p_\infty - p_u \uparrow \quad p_u \downarrow .$$

Similarly, on the lower surface,

$$\tau \uparrow \quad R \uparrow \quad \frac{\partial p}{\partial r} = \rho \frac{V^2}{R} \downarrow \quad p_l - p_\infty \downarrow \quad p_l \downarrow .$$

Since the addition of thickness to a cambered airfoil tends to lower both the upper and lower surface pressure and the lift is an integral of the upper and lower surface pressure difference, the resulting lift will be relatively unaffected by thickness. These trends in c_p and c_l can be observed by comparing the 10% thick cambered airfoils shown in Figures 7 and 8 to the 2% thick cambered airfoils shown in Figures 3 and 4. Note: the thicker airfoils were simulated at the same angles of attack for the corresponding thinner airfoils. For these conditions, the 5 times increase in thickness from 2% to 10% changes the lift by less than 10%.

XFOIL
V 6.95

NACA 4502
α = -0.0984°
C_L = 0.5000
C_M = -0.1260
C_{Dp} = -0.00127

Figure 3: NACA 4502, $c_l = 0.5$.

XFOIL
V 6.95

NACA 4202
α = 0.8560°
C_L = 0.5000
C_M = -0.0736
C_{Dp} = -0.00199
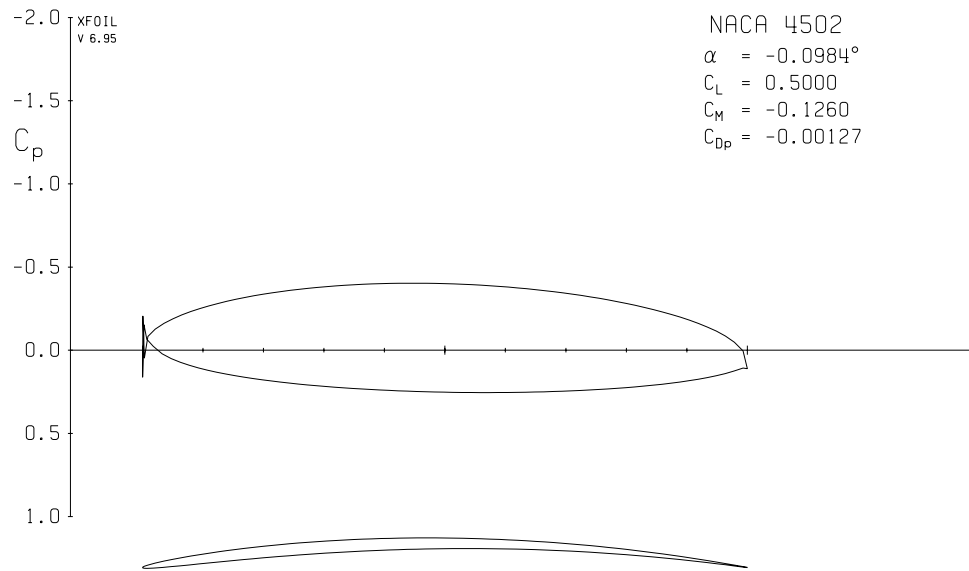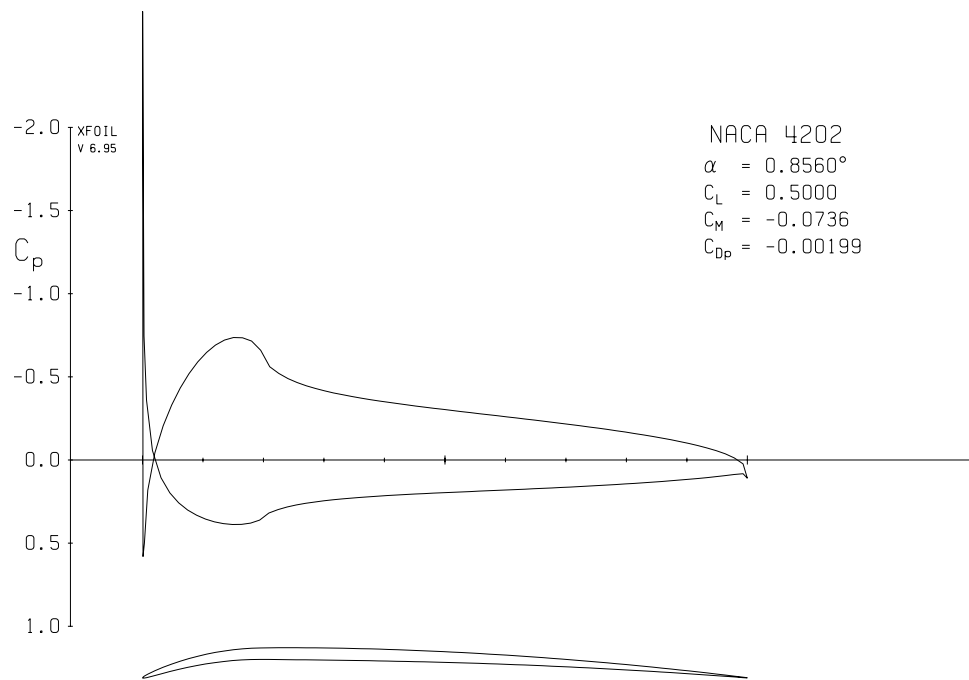
Figure 4: NACA 4202, $c_l = 0.5$.

4
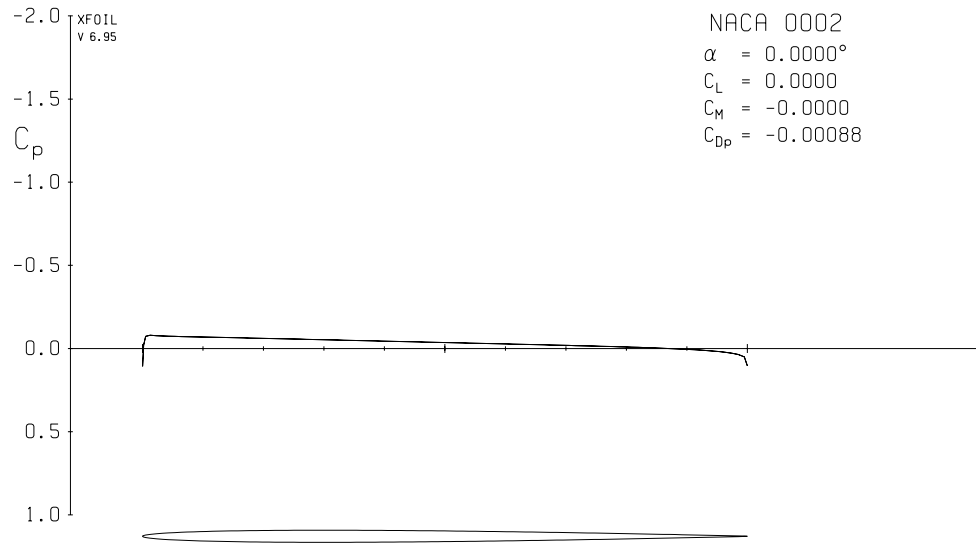
Figure 5: NACA 0002, $\alpha_\infty = 0°$.

Figure 6: NACA 0010, $\alpha_\infty = 0°$.

XFOIL
V 6.95

NACA 4510
α = -0.0984°
C_L = 0.5383
C_M = -0.1308
C_{Dp} = -0.00095
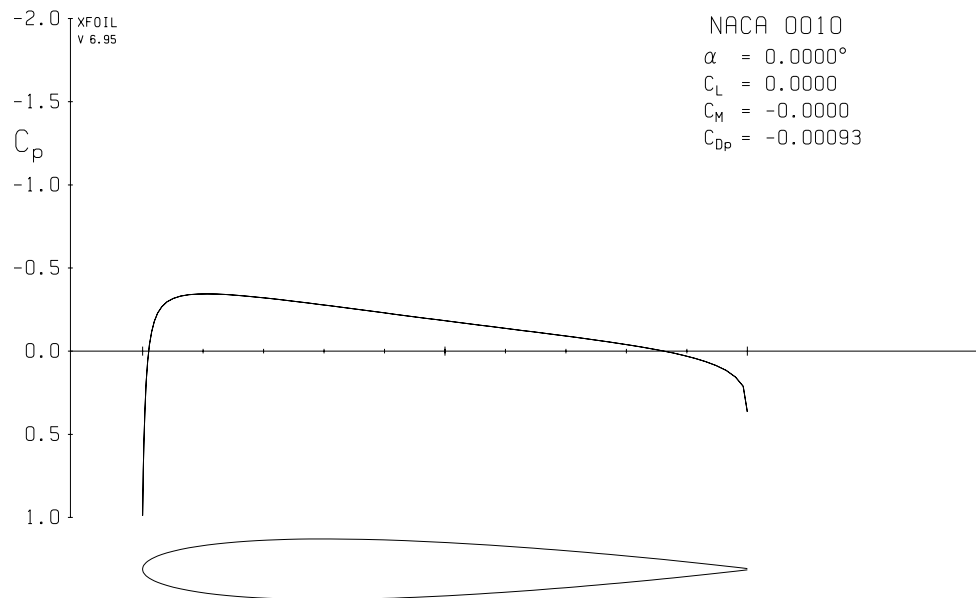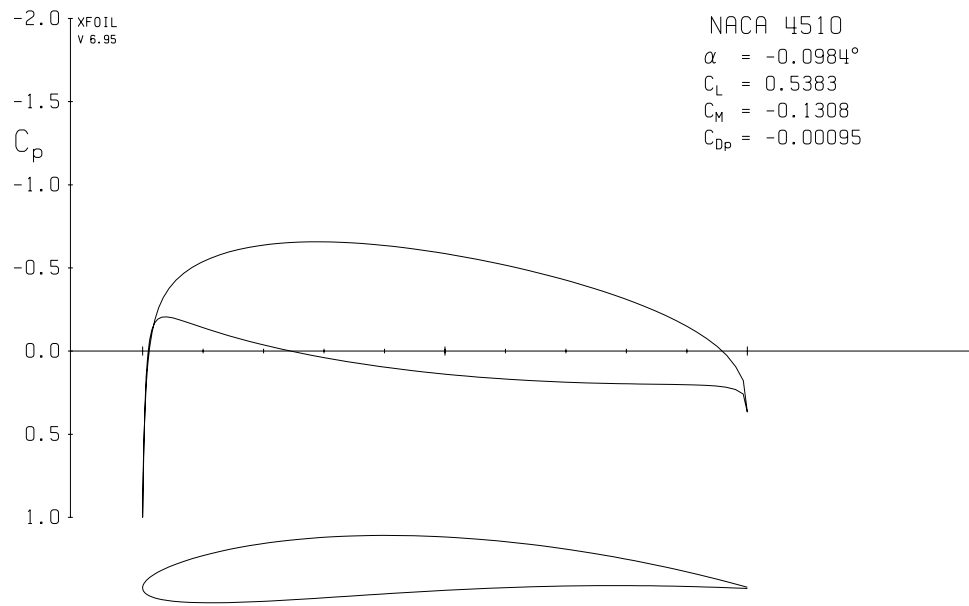
Figure 7: NACA 4510, $\alpha_\infty = -0.09854°$.

XFOIL
V 6.95

NACA 4210
α = 0.8560°
C_L = 0.5399
C_M = -0.0760
C_{Dp} = -0.00100
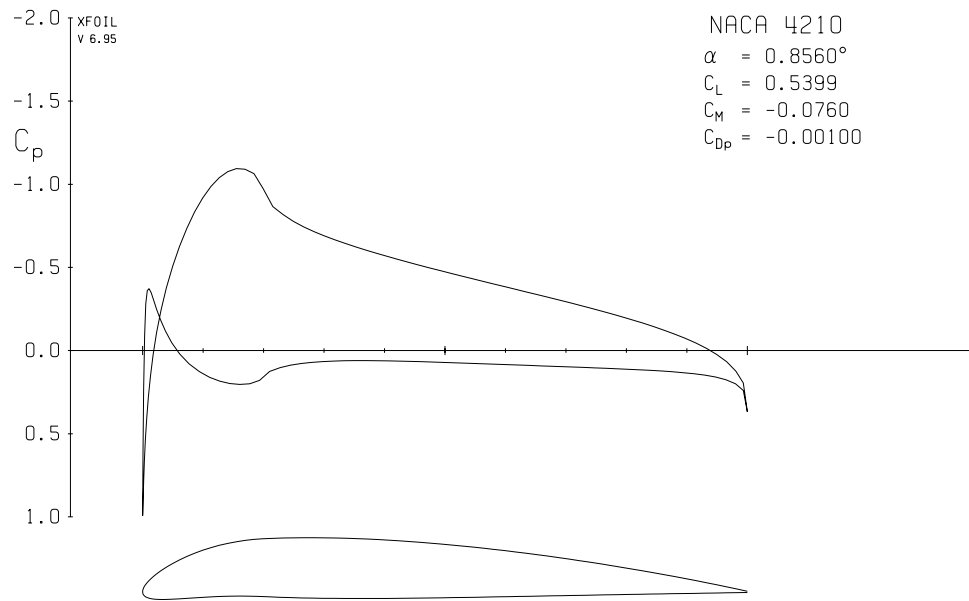
Figure 8: NACA 4210, $\alpha_\infty = 0.856°$.

6

5   Leading-edge Behavior

Next, we will consider the behavior of the flow at the leading edge. As was noted above, the flow will stagnate near the leading edge which results in $c_p = 1$. However, another effect often results in very low pressures at the leading edge. For example, the c_p distribution around the NACA 4202 airfoil at $c_l = 0.5$ shows $c_p < -2$ at the leading edge. The cause of this can be explained also through the streamline curvature argument. In this case, the radius of curvature at the leading edge is very small. And, as $R \to 0$,

$$\lim_{R \to 0} \frac{\partial p}{\partial r} = \rho \frac{V^2}{R} \to \infty.$$

Thus, the pressures at the leading edge will need to be very low to provide the required force to turn the flow around the leading edge.

Question: Figure 4 and Figure 9 show the c_p distributions for the NACA 4202 and NACA 0002, respectively, for $c_l = 0.5$. Is the leading-edge stagnation point on the lower surface or upper surface for the NACA 4202? What about the NACA 0002?

Question: Explain the differences in the c_p behavior at the leading edge for the NACA 4202 and 4210 airfoils.

Figure 9: NACA 0002, $cl = 0.5$.